



HAL
open science

Quality of the strain state in simple shear testing using field measurement techniques

Baptiste Reyne, Diane Hérault, Sandrine Thuillier, Pierre-Yves Manach

► To cite this version:

Baptiste Reyne, Diane Hérault, Sandrine Thuillier, Pierre-Yves Manach. Quality of the strain state in simple shear testing using field measurement techniques. *International Journal of Mechanical Sciences*, 2021, 208, pp.106660. 10.1016/j.ijmecsci.2021.106660 . hal-04693465

HAL Id: hal-04693465

<https://ubs.hal.science/hal-04693465v1>

Submitted on 13 Nov 2024

HAL is a multi-disciplinary open access archive for the deposit and dissemination of scientific research documents, whether they are published or not. The documents may come from teaching and research institutions in France or abroad, or from public or private research centers.

L'archive ouverte pluridisciplinaire **HAL**, est destinée au dépôt et à la diffusion de documents scientifiques de niveau recherche, publiés ou non, émanant des établissements d'enseignement et de recherche français ou étrangers, des laboratoires publics ou privés.



Distributed under a Creative Commons Attribution - NonCommercial 4.0 International License

Quality of the strain state in simple shear testing using field measurement techniques

Baptiste Reyne^{a,*}, Diane Herault^a, Sandrine Thuillier^a, Pierre-Yves Manach^a

^a*Univ. Bretagne Sud, UMR CNRS 6027, IRDL, F-56100 Lorient, France*

Abstract

Shear testing holds a peculiar place in sheet metal characterization for multiple reasons. Indeed, as opposed to tension or bi-axial expansion, the principal strains of such a deformation change their direction, non-linearly, as a test proceeds. It is, in general, also impossible for an experimental setup to reproduce theoretical conditions. The kinematics assumptions are therefore not verified in absolute, but satisfied up to a certain level that often remains subjective. Fortunately, field measurement methods provide comprehensive data that can be used for assessing and improving experimental processing. In this work, digital image correlation is applied to different types of shear testing performed on a dual phase steel. Results are used to construct quantitative estimators to assess the quality of measurement as well as to decrease the number and weight of assumptions. A method is also proposed to separate the measured kinematics into the expected theoretical ones and the unwanted experimental deviations. It is quantitatively shown that, for the considered material and sample types, translational simple shear testing achieves kinematics that are closer to theory than pseudo-simple shear testing. The other major finding of this work is a method to identify shear strains independently of experimental biases.

Keywords: simple shear, characterization, sheet metals, field measurement techniques,

*Corresponding author.

Email address: breyne@postech.ac.kr (Baptiste Reyne)

Contents

1	Introduction	3
2	Material and methods	5
3	Theory and calculation	6
3.1	Kinematics	6
3.1.1	Simple shear deformation	6
3.1.2	Post-processing approaches	10
3.1.3	Deviation from simple shear kinematics	11
3.1.4	Heterogeneity	13
3.2	Sthenics	14
3.2.1	Shear stresses standard identification	14
3.2.2	Consistent lagrangian stress	15
3.2.3	Consistent eulerian stress	15
3.2.4	Momentum balance	16
4	Results and discussion	17
4.1	Shear parameter identification	17
4.2	Deviation from simple shear	18
4.3	Heterogeneity	22
4.4	Stress correction	22
4.5	Work-hardening	23
5	Conclusions	24
Appendix A	Shear deformation identities	26

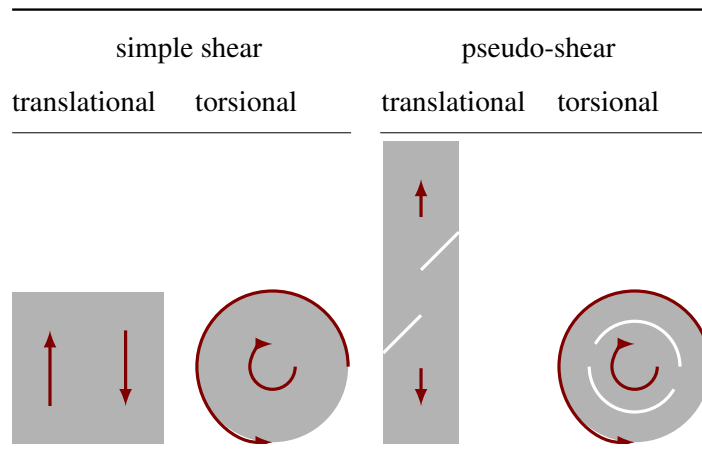


Figure 1: Illustrative definitions of the different shear testing technologies. Gray areas represent the sample geometries while arrows indicate the imposed kinematics.

1. Introduction

Sheet metals represent a capital basic resource in manufacturing industries. Their forming requires complex processes involving a wide variety of mechanical phenomena. Among them: plasticity with potential rate dependence, finite deformations, damage or fracture. Moreover, the production of sheet metals includes several steps of rolling at different temperature levels which act on the poly-crystalline structure. This necessarily alters the geometry and orientations of grains hence exacerbates their macroscopic anisotropy.

Because of plastic anisotropy, the classical tensile test alone is no longer sufficient. The pursuit of a thorough material characterization therefore demands to explore a wider range of plane stress directions. For example, simple shear testing is used in the literature to calibrate the yield surfaces of anisotropic materials as studied and applied by Vegter and van den Boogaard (2006); Zang et al. (2011); Abedini et al. (2017, 2018). Shear testing can also bring important experimental advantages such as large strains or reverse loading possibilities. This type of testing can be achieved by several means that types are presented in figure 1. They are first distinguished in terms of loading path (translational or torsional) and then depending on the application of boundary conditions. Simple shear refers to the case where the displacements of the gauge zone boundaries are imposed to match the shear theoretical motion. Pseudo-shear designates the case where the displacements are not prescribed directly, but resulting shear forces are expected at the gauge zone boundaries.

Translational simple shear (Miyachi, 1977; An et al., 2009; Manach et al., 2014) is a straightforward way to materialize a shear load onto sheet metals. It gives important possibilities such as reverse loading

20 (Carbonnière et al., 2009) or anisotropy characterization (Rauch, 1998; Lou et al., 2020), that importance in metal forming have been acknowledged for several decades (Courbon and Duval, 1993). It nevertheless demands a rigid setting with severe geometrical restriction on the samples in order to avoid buckling (Pham et al., 2017) or critical heterogeneities (G' Sell et al., 1983; Bouvier et al., 2006). Stresses tend to concentrate at the grips locations which hinders fracture characterization. Translational pseudo-simple shear (refereed
25 to as pseudo-shear) (Mohr and Henn, 2004; Reyes et al., 2009; Shouler and Allwood, 2010; Roth and Mohr, 2016; ASTM, 2019) decreases the stiffness of the setup, reduces kinematic gradients and opens to a more reliable fracture characterization (Abedini et al., 2016; Zhang et al., 2019). It unfortunately loses some advantages of simple shear such as the possibility of reverse loading. An important issue also subsists in the stress concentration and necessary heterogeneities obtained at the edges of the sample. An elegant
30 way to suppress this problem is to consider a setup without edges: torsional simple shear (Marciniak and Kolodziejwski, 1972; Yin et al., 2015). This is the only shear technology that can provide a uniform loading. But the area that resists to the imposed torque revolves around all directions of the sample, which makes it impossible to distinguish any anisotropic effect in sheet metals. To that end, torsional pseudo-shear (Brosius et al., 2011; Yin et al., 2012, 2014) only acts on two parallel and opposed bridges that material orientation is
35 unique and controlled. With the reintroduction of edges, it is nevertheless subjected to difficulties similar to translational pseudo-shear. In addition, mixed strain paths can be explored using tension–shear combined setups (Kumar et al., 2020; Wang et al., 2020) or multi-step characterization (Bouvier et al., 2006; Starman et al., 2019). A number of other hybrid or alternative specimens have been introduced and adopted in the literature, such as the butterfly-type (Mohr and Henn, 2007) that was designed to allow different levels of
40 triaxiality. These have become necessary in the calibration of anisotropic hardening models (Barlat et al., 2020; Hérault et al., 2021) for the prediction of forming processes.

It is clear from the last paragraph that shear technologies all come with advantages and drawbacks. For a given material, they should all lead to identical results which cannot always be achieved as shown by Yin et al. (2014). Heterogeneities and edge effects have been characterized and quantified in several
45 studies (G' Sell et al., 1983; Bouvier et al., 2006). As emphasized by Roth and Mohr (2018), the premature tensile fracture they provoke limits the validity of shear characterization. The corresponding rotation of the material frame (Moreira and Nunes, 2013; Abedini et al., 2020) and the presence of normal stresses (Pereira et al., 2019; Abedini et al., 2020) can also bring significant variations in post-processed results. According to Mazière et al. (2017) in the case of plastic instabilities, the very tightening of grips may reflect on the

50 measured behavior. The approximated stress states and their consistency with the chosen strains remain a non trivial matter discussed in several analyses (Zhou and Tamma, 2003; Destrade et al., 2012; Butcher and Abedini, 2017; Thiel et al., 2019). For these reasons, the study of shear testing techniques is an ongoing field of research on both the experimental and theoretical sides. To tackle some of these issues, the experimental measurement of strains has been improved by several means. For instance, Thuillier and Manach (2009) 55 make use of a point tracking method combined with a principal strains formulation to identify a shear strain measure. Advances in field measurement techniques such as digital image correlation (DIC) also bring strong advantages to the understanding of experimental kinematics. An important part of today's results (Yin et al., 2014; Manach et al., 2014) is owed to such techniques. At a given instant, a single gauge or extensometer may only provide one component of a strain tensor averaged over a small area. In the mean 60 time, field measurement techniques allow to estimate every planar component of a strain measure over an entire area. Possible heterogeneities and unwanted (theoretically absent but experimentally unavoidable) deformations can be revealed.

Hence the purpose of this work is to use kinematic field measurements to address several ongoing questions regarding shear testing. With the full knowledge of in-plane kinematics, assumptions can be 65 weakened, definitions specified and errors quantified. After a recall on the theory of simple shear and the standard postprocessing of experiments, a new method is proposed to lift ambiguities in the definition of the shear parameter. It relies on an explicit partition of the measured deformation gradient into a theoretical contribution and an unwanted one. These quantities are then used to derive homogeneity and error estimators, as well as consistent stresses definitions. These methods are finally applied to compare different shear 70 experimental setups with an advanced high strength steel.

2. Material and methods

The experimental setups considered in this paper are illustrated in figure 2 while the geometries of shear testing specimens are detailed in figure 3. The material is a high strength dual phase steel (DP600) laminated in sheets of thickness 1.2 mm. Shear testing technologies are implemented on a tensile machine 75 with cell capacities 50 kN (samples s1, s2, p2) and 10 kN (samples p1). The specimens are loaded along their rolling direction. In order to obtain the strains components, images are acquired and postprocessed with the Gom–Aramis system that uses a subset-based digital image correlation algorithm. The facet size ranges from 10 to 15 pixels, which corresponds to a physical size of 0.1 mm to 0.2 mm. No regularization

was used in the image processing. The forces measured by the different load cells are used to calculate the stresses.

Firstly, the simple shear setup (figure 2-s) is composed of two grips which apply a clamping force on the specimen of 10 kN to 15 kN to avoid the sliding of the specimen. One of the grips is fixed and a vertical displacement is applied on the other one. It is not possible to obtain fracture considering the stiffness of this setup whereas it is possible with pseudo-shear geometries which are fixed with a system of pins. In fact the bottom pin is fixed and a vertical displacement is applied on the top one (figure 2-p) but the area of interest in the center is not impacted directly by the boundary conditions.

There are four translational shear samples as shown in figure 3: two variants of simple shear labelled s1 and s2, and two variants of pseudo-shear labelled p1 and p2. The two simple shear specimens s1 and s2 have a rectangular shape but there are circular arcs machined at each extremity s2 that are intended to reduce edge effects during the test. The shear direction is vertical along the length of the specimen and the width between the grips is 4 mm. The two others geometries have more complex shapes including two symmetric regions of interest with a consequent reduction of the length compared to simple shear specimens.

3. Theory and calculation

3.1. Kinematics

3.1.1. Simple shear deformation

This section summarizes analytical results from the definition of simple shear to the derivation of several tensors of interest. The considered body occupies an initial configuration Ω_0 ; its deformation is described by a mapping \mathbf{y} to its current configuration Ω . *Simple shear* hereafter refers to a deformation that can be written in the form:

$$\begin{aligned} \mathbf{y} : \Omega_0 &\longrightarrow \Omega \\ \mathbf{X} &\longmapsto \mathbf{y}(\mathbf{X}) = X_1 \mathbf{e}_1 + (X_2 + \gamma X_1) \mathbf{e}_2 + X_3 \mathbf{e}_3. \end{aligned} \quad (1)$$

Let $\mathbf{b} = (\mathbf{e}_1, \mathbf{e}_2, \mathbf{e}_3)$ be the associated direct orthonormal cartesian basis that will be used throughout this work. The simple shear deformation is illustrated in figure 4 for a rectangular body of initial plane dimensions $l \times h$, that right edge is vertically displaced of $d = h\gamma$.

The *shear parameter* γ is the single variable that characterizes such a deformation. The consecutive

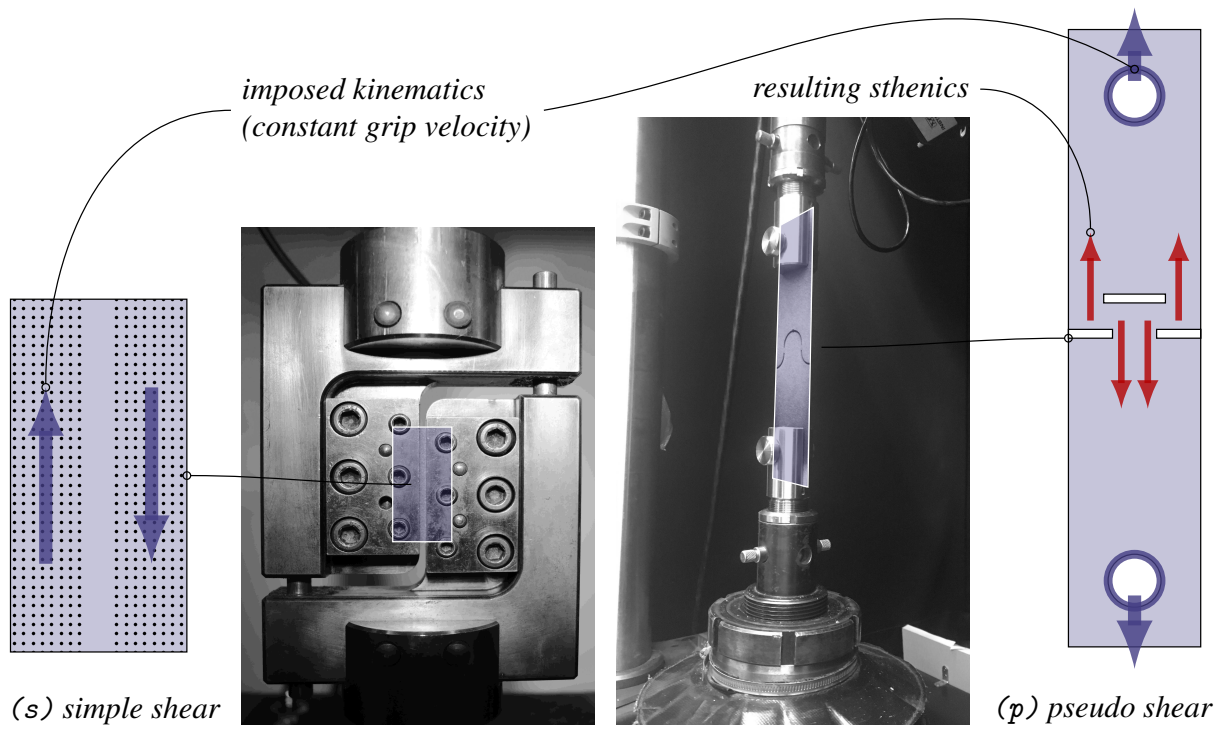


Figure 2: Experimental setups for simple shear (dedicated equipment) and pseudo-shear (tensile apparatus). In both cases the boundary conditions are a constant grip velocity. In the case of pseudo-shear, the geometry ensures resulting shear forces in the gauge zone. The present illustration is purely schematic: geometric details are provided in figure 3.

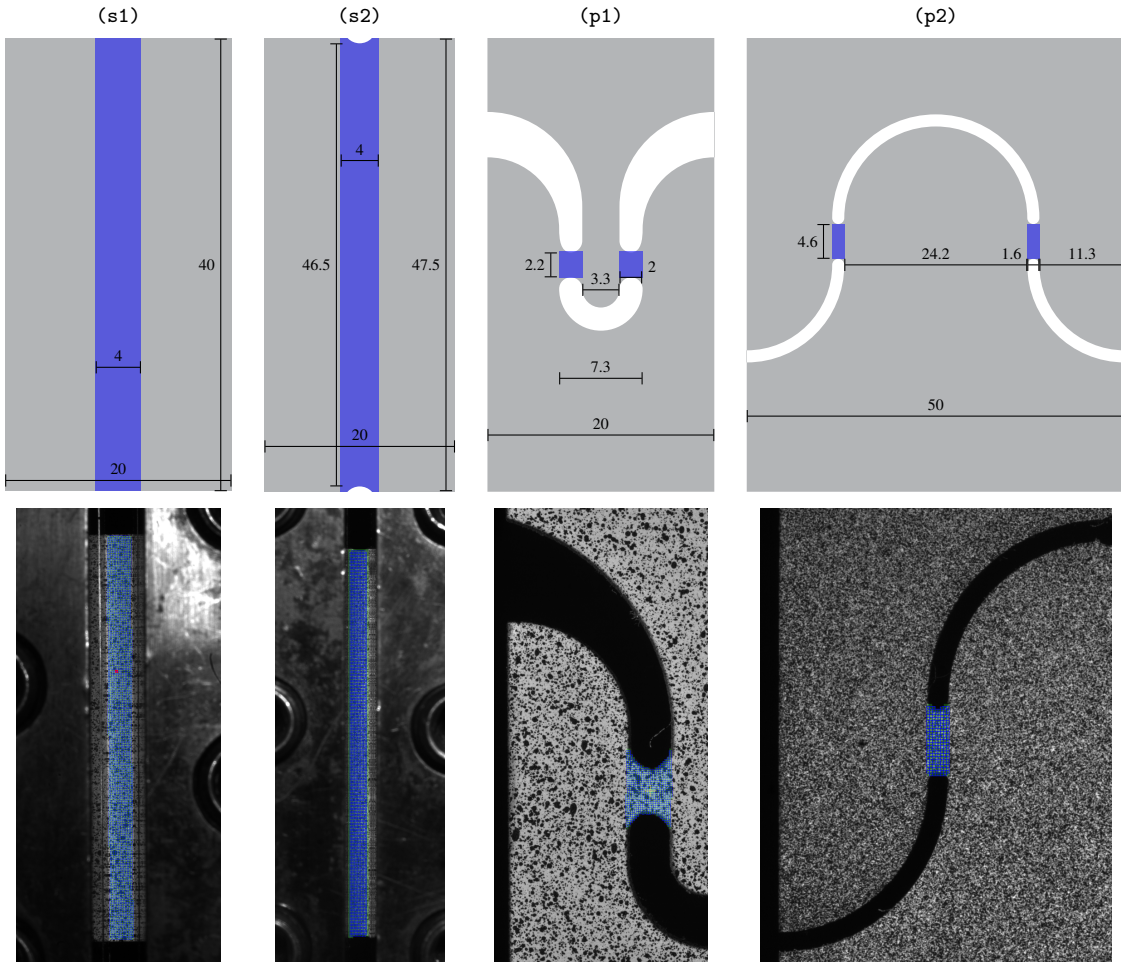


Figure 3: Considered geometries for shear testing with units in mm. Label “s” refers to *simple* shear while “p” refers to *pseudo*-shear. s1 and s2 are variants of the modified Miyaushi test, while p1 is inspired by Roth and Mohr (2016) and p2 is defined by Shouler and Allwood (2010). The bottom row presents in situ pictures with DIC grids depicted in blue that cover the gauge zones.

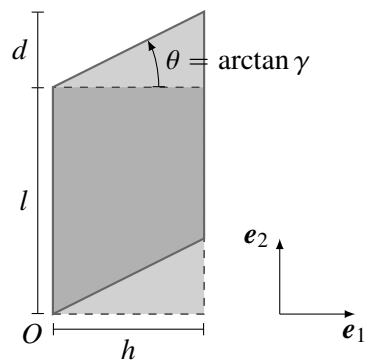


Figure 4: Simple shear kinematics in the common frame of reference (e_1, e_2) . The right vertical edge is vertically displaced over a distance $d = h\gamma$, where γ is called *shear parameter*.

deformation gradient \mathbf{F} , right Cauchy–Green measure \mathbf{C} and Green–Lagrange strain \mathbf{E} yield respectively:

$$\mathbf{F} = \text{grad } \mathbf{y} = \mathbf{I} + \gamma(\mathbf{e}_2 \otimes \mathbf{e}_1); \quad (2)$$

$$\mathbf{C} = \mathbf{F}^\top \mathbf{F} = \mathbf{I} + \gamma^2(\mathbf{e}_1 \otimes \mathbf{e}_1) + 2\gamma \text{sym}(\mathbf{e}_1 \otimes \mathbf{e}_2); \quad (3)$$

$$\mathbf{E} = \frac{1}{2}(\mathbf{C} - \mathbf{I}) = \frac{\gamma^2}{2}(\mathbf{e}_1 \otimes \mathbf{e}_1) + \gamma \text{sym}(\mathbf{e}_1 \otimes \mathbf{e}_2); \quad (4)$$

where the symmetric part operator reads $\text{sym } \bullet = (\bullet + \bullet^\top)/2$ and \mathbf{I} is the second order tensorial identity.

The eigenvalues problem applied to the Cauchy–Green tensor leads to solutions of the form:

$$\mathbf{C} = C_1 \mathbf{V}_1 \otimes \mathbf{V}_1 + C_2 \mathbf{V}_2 \otimes \mathbf{V}_2 + \mathbf{e}_3 \otimes \mathbf{e}_3 \quad (5)$$

$$\text{where } C_1 = 1 + \frac{\gamma}{2} \left(\gamma + \sqrt{4 + \gamma^2} \right), \quad (6)$$

$$C_2 = 1 + \frac{\gamma}{2} \left(\gamma - \sqrt{4 + \gamma^2} \right); \quad (7)$$

$$\text{and } \mathbf{V}_1 \propto 2\mathbf{e}_2 + \left(\gamma + \sqrt{4 + \gamma^2} \right) \mathbf{e}_1, \quad (8)$$

$$\mathbf{V}_2 \propto -2\mathbf{e}_1 + \left(\gamma + \sqrt{4 + \gamma^2} \right) \mathbf{e}_2, \quad (9)$$

$$\|\mathbf{V}_1\| = \|\mathbf{V}_2\| = 1. \quad (10)$$

100 In the expressions above, \propto indicates proportionality. Note that the eigendirections are nonlinear functions of the shear parameter.

The polar decomposition of the deformation gradient reads $\mathbf{F} = \mathbf{R}\mathbf{U}$ where \mathbf{R} is an orthogonal tensor (a rotation) and \mathbf{U} the right stretch tensor. Since $\mathbf{C} = \mathbf{U}^\top \mathbf{U}$, the stretch eigenvalues can be obtained directly:

$$\mathbf{U} = U_1 \mathbf{V}_1 \otimes \mathbf{V}_1 + U_2 \mathbf{V}_2 \otimes \mathbf{V}_2 + \mathbf{e}_3 \otimes \mathbf{e}_3 \quad (11)$$

$$\text{where } U_1 = \sqrt{C_1} = \frac{1}{2} \left(\sqrt{4 + \gamma^2} + \gamma \right), \quad (12)$$

$$U_2 = \sqrt{C_2} = \frac{1}{2} \left(\sqrt{4 + \gamma^2} - \gamma \right). \quad (13)$$

As can be found in the literature (Salomon, 2011, page 228), the golden ratio $\varphi = (1 + \sqrt{5})/2$ arises for a unitary shear, that is when $\gamma = 1$ or $\theta = \pi/4$. In this case, one finds $U_1 = \varphi$ and $U_2 = 1/\varphi = \varphi - 1$. This means that during such a deformation, shapes are stretched by the golden ratio in their initial \mathbf{V}_1 direction
105 and compressed by the golden ratio in their initial direction \mathbf{V}_2 .

The expression of the right stretch in the reference basis can be obtained by substituting the eigenvectors expressions in favor of $(\mathbf{e}_1, \mathbf{e}_2)$. A far easier way is to use a direct formula to compute the square root of \mathbf{C}

in the reference basis. The result yields

$$\mathbf{U} = \frac{2}{\sqrt{4 + \gamma^2}} \left(\left(1 + \frac{\gamma^2}{2} \right) \mathbf{e}_1 \otimes \mathbf{e}_1 + \mathbf{e}_2 \otimes \mathbf{e}_2 + \gamma \text{sym}(\mathbf{e}_1 \otimes \mathbf{e}_2) \right) + \mathbf{e}_3 \otimes \mathbf{e}_3. \quad (14)$$

The rotation is obtained by computing

$$\mathbf{R} = \mathbf{F}\mathbf{U}^{-1} = \frac{1}{\sqrt{4 + \gamma^2}} (2\mathbf{I} + \gamma(-\mathbf{e}_1 \otimes \mathbf{e}_2 + \mathbf{e}_2 \otimes \mathbf{e}_1)). \quad (15)$$

Finally, the Hencky (or logarithmic) spatial strain measure, further denoted \mathbf{h} , is of interest for constitutive modeling since it is the work-conjugate of the Cauchy stress, provided that a corotational frame of reference is used. It is obtained by first computing the material Hencky strain that yields in the eigenbasis:

$$\mathbf{H} = \ln \mathbf{U} = \ln U_1 \mathbf{V}_1 \otimes \mathbf{V}_1 + \ln U_2 \mathbf{V}_2 \otimes \mathbf{V}_2 \quad (16)$$

$$\text{where } \ln U_1 = -\ln U_2 = \sinh^{-1}(\gamma/2). \quad (17)$$

This convenient equivalence with the inverse hyperbolic sine function is used by Butcher and Abedini (2017). Since the material and spatial logarithmic strains share the same eigenvalues, a rotation yields

$$\mathbf{h} = \mathbf{R}\mathbf{H}\mathbf{R}^\top = \frac{\sinh^{-1}(\gamma/2)}{\sqrt{4 + \gamma^2}} (-\gamma \mathbf{e}_1 \otimes \mathbf{e}_1 + \gamma \mathbf{e}_2 \otimes \mathbf{e}_2 + 4 \text{sym}(\mathbf{e}_1 \otimes \mathbf{e}_2)). \quad (18)$$

In order to derive these expressions, helpful identities are recalled in Appendix A.

3.1.2. Post-processing approaches

This short section recalls the different approaches used to quantify the motion after experimental results; it motivates the complements introduced further in the paper. The simple shear parameter is the natural quantity of interest since it defines the motion straightforwardly. An approximation of it can be obtained by several means. For instance, a global estimate of the shear parameter can first be computed as d/h (figure 4) where d is taken as the grips displacements (Rauch, 1998; Bouvier et al., 2006; Khan et al., 2011).

Since global measurements can be subjected to a number of experimental biases, local estimates are preferred as in Garcia et al. (1980) where the shear parameter $\gamma = 2E_{12}$ is computed from the Green-Lagrange strain measured with strain gauges. For identifying constitutive models, a number of studies directly use the spatial Hencky component h_{12} from measurements which is comparable to the previous approach. Translational simple shear was developed and applied to metallic thin sheet materials, e.g. Rauch and G'Sell (1989), using a local measure of the displacement in the shear direction, using a straight line recorded in real-time with a camera. Full-field measurements give the strain distribution over the entire gauge length, and a fairly homogeneous distribution is highlighted by Zang et al. (2011).

In order to emancipate from rotations between frames of reference, tensors invariants can be used. For example, the shear parameter utilized by (Thuillier and Manach, 2009) comes from a combination of eigenvalues of the Almansi measure. Since this approach is performed in the eigenbasis, a potential drawback is that the rotations of the body are not accounted for. Therefore the orientation of the sample cannot be guaranteed in absolute for an anisotropic identification.

With modern technologies, strain components are classically obtained from an average value computed on a homogeneous zone using field measurements techniques. These approaches are compared in section 4.1.

3.1.3. Deviation from simple shear kinematics

Local estimates based on strain measures (described in section 3.1.2) make one common hypothesis: the measured deformation is simple shear. In other words, it is postulated that the experimental deformation field can be put in the form of equation (1). Also, since simple shear exhibits two different eigenvalues, the shear parameter identification can always be performed on at least two components of the measured strain. However, the measured deformation is never simple shear alone. Therefore, the shear parameter cannot be uniquely defined using local strain estimates. This fact is illustrated by the results of section 4.1.

In order to exactly and uniquely distinguish the different contributions in the measured deformation, the following multiplicative decomposition is proposed.

$$\overbrace{\begin{bmatrix} F_{11}^m & F_{12}^m \\ F_{21}^m & F_{22}^m \end{bmatrix}}_{\mathbf{F}^m} = \underbrace{\begin{bmatrix} \cos \mu & -\sin \mu \\ \sin \mu & \cos \mu \end{bmatrix}}_{\mathbf{R}^*} \underbrace{\begin{bmatrix} u_1 & 0 \\ 0 & u_2 \end{bmatrix}}_{\mathbf{U}^*} \overbrace{\begin{bmatrix} 1 & 0 \\ \gamma & 1 \end{bmatrix}}_{\mathbf{F}^s}, \quad (19)$$

where \mathbf{F}^m is the measured deformation gradient split into: a theoretical shear contribution \mathbf{F}^s , and an unwanted contribution \mathbf{F}^* . The latter is decomposed into an unwanted stretch \mathbf{U}^* and an unwanted rotation \mathbf{R}^* . The multiplicative decomposition of the deformation gradient is a tool used in several anelastic constitutive theories. It is here applied to experimental data. Thuillier and Manach (2009) already investigated shear kinematics enriched with one parameter. The present enrichment with three parameters encompasses all possible plane deformations.

Since the operation is not commutative, the order of the two contributions (illustrated in figure 5) must be justified. In the proposed formulation, the theoretical contribution is applied first on the initial configuration;

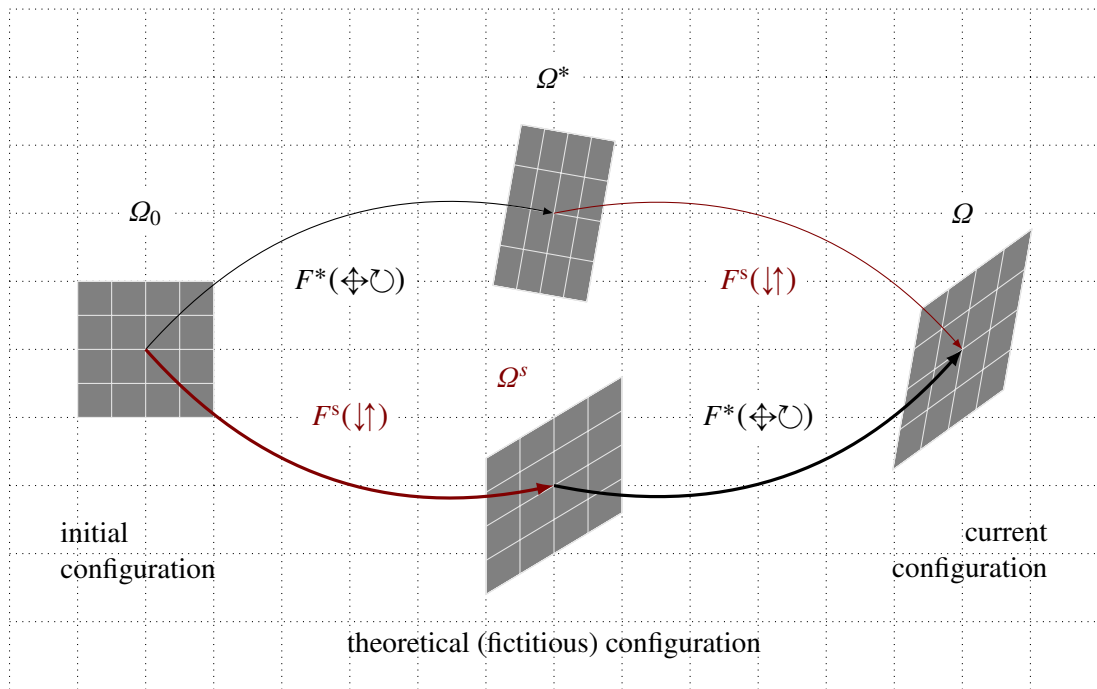


Figure 5: Possible decompositions of the measured deformation gradient. In the top case $F^m = F^s F^*$, the theoretical shear is applied after the unwanted deformation. Therefore it is not aligned with the initial orientation of the sample. In the bottom case $F^m = F^* F^s$, the theoretical shear is applied first on the initial configuration that is controlled by the operator, hence its consistency with the shear characterization purpose.

then the unwanted contribution brings the effective simple shear to the current (measured) configuration with a stretch and a rotation. This way, the simple shear is computed on the configuration that is adjusted by the operator, with controlled placement and alignment. It is specifically relevant when the anisotropy of the material is characterized. Had the unwanted contribution been applied first, the computed simple shear
150 would correspond to a possibly rotated and stretched body, in spite of the operators' efforts to correctly place and align the sample and the equipment.

Expression (19) provides four scalar independent equations with four unknown parameters μ (unwanted rotation angle), u_1 , u_2 (unwanted stretches) and γ . It can describe any admissible two-dimensional deformation and permits to separate its different contributions. Solving it leads to:

$$\gamma = \frac{F_{11}^m F_{12}^m + F_{21}^m F_{22}^m}{F_{12}^{m2} + F_{22}^{m2}}, \quad (20)$$

$$u_1 = \frac{F_{11}^m F_{22}^m - F_{12}^m F_{21}^m}{\sqrt{F_{12}^{m2} + F_{22}^{m2}}}, \quad (21)$$

$$u_2 = \sqrt{F_{12}^{m2} + F_{22}^{m2}}, \quad (22)$$

$$\tan \mu = \frac{-F_{12}^m}{F_{22}^m}. \quad (23)$$

These quantities yield a robust and unambiguous definition that interpretation is straightforward. In the ideal case, $F_{11}^m = F_{22}^m = 1$, $F_{12}^m = 0$ and $F_{21}^m = \gamma$. The corresponding unwanted deformation gradient reduces to unity and one finds $\mathbf{F}^s = \mathbf{F}^m$. When an unwanted deformation is introduced, it can be quantified
155 in terms of the rotation angle μ and unwanted stretches u_1 and u_2 .

3.1.4. Heterogeneity

As detailed in section 3.1.2, homogeneity is a critical assumption in the postprocessing of shear testing. There is a need to quantitatively estimate a distance to homogeneity for each test in order to compare, validate or discriminate them. The proposed estimator is named heterogeneity factor and given by:

$$s(X_1, t) = \sqrt{\int_0^l \left(\frac{\gamma - \bar{\gamma}}{l} \right)^2 dX_2}, \quad (24)$$

with the average along the loaded section:

$$\bar{\gamma}(X_1, t) = \int_0^l \gamma dX_2, \quad (25)$$

where the unique γ is defined in equation (20). This is a standard deviation of the shear parameter distribution, along the longitudinal axis (parallel to the shear force), at fixed transversal coordinate. It is important

that the function remains variable with X_1 such that it is not affected by lateral boundary conditions that would complicate any comparison between simple and pseudo-shear. The X_1 coordinate also maps to a longitudinal section of the material where the mechanical equilibrium is computed to obtain a stress estimation. It also matters that the function is unitless so that different geometries and aspect ratios can be compared. The standard deviation is here a natural choice since it quantifies a distance to average which is the value that is classically taken to represent the whole strains distribution.

3.2. Sthenics

3.2.1. Shear stresses standard identification

Stress states are much harder to access than any kinematic measure since the only available data usually come from one force sensor, that value is denoted f . The standard approach consists in postulating the form

$$\boldsymbol{\sigma} = 2\tau \text{sym}(\mathbf{e}_1 \otimes \mathbf{e}_2) \quad (26)$$

for the Cauchy stress tensor, homogeneous on the sample. In this expression, τ is called the shear stress and chosen as sthenic quantity of interest. Several works (G' Sell et al., 1983; Garcia et al., 1980; Bouvier et al., 2006) show that normal stresses are always present by means of mechanical balance, but can be neglected when the ratio h/l is *small enough*. This means that the forces acting on the sample are assumed to be purely shear along the loading direction. Then writing the momentum balance of a planar section A of normal \mathbf{e}_1 yields:

$$\mathbf{f} = f\mathbf{e}_2 = \int_A \boldsymbol{\sigma}\mathbf{e}_1 \, dA. \quad (27)$$

Note that this expression also implies that the resulting force is assumed to be purely vertical. By means of homogeneity and assuming a perfect match with theoretical kinematics (i.e. the initial section remains vertical with unchanged area), the integral simplifies and one finds

$$\tau = f/A_0, \quad (28)$$

where A_0 is the initial cross-sectional area of the sample.

But the assumptions of perfect alignment and theoretical shear deformations are no longer needed when field measurement techniques can quantify any deviation. The remaining challenge is therefore to find an appropriate stress measure that fits with the proposed theoretical shear parameter identification. In the following sections, consistent stress measures are derived as the work-conjugates of the theoretical contribution to the effective motion. Then the momentum balance is revisited to allow their identification.

3.2.2. Consistent lagrangian stress

The shear parameter γ is the lagrangian kinematic quantity of interest. Its conjugate scalar stress is derived below. The power of internal forces developed in a material element of the initial configuration $d\Omega_0$ reads

$$p_i = J\mathbf{II} : \dot{\mathbf{F}} \quad (29)$$

where $J = \det \mathbf{F}$ is the deformation jacobian and \mathbf{II} the first Piola–Kirchhoff stress tensor. Under the assumption of isochoric deformation in elasto-plasticity, it is assumed to be unity. Applied to the measured deformation and using the multiplicative decomposition ($\mathbf{F} = \mathbf{F}^m = \mathbf{F}^* \mathbf{F}^s$), the previous expression can be split into a theoretical part and an *unwanted* contribution.

$$p_i = \underbrace{(\mathbf{II} \mathbf{F}^{s\top}) : \dot{\mathbf{F}}^*}_{p_i^*} + \underbrace{(\mathbf{F}^{*\top} \mathbf{II}) : \dot{\mathbf{F}}^s}_{p_i^s}. \quad (30)$$

The terms under parentheses refer to stress measures that conjugate with, respectively, the unwanted and theoretical motions. They can be computed from measurements given the knowledge of \mathbf{II} . Substituting tensors for their expressions in the reference basis, the theoretical part of the power of internal forces reads

$$p_i^s = \underbrace{(\Pi_{11} u_1 \sin \mu + \Pi_{21} u_2 \cos \mu)}_{\Pi_{21}^s} \dot{\gamma}. \quad (31)$$

In the above, Π_{21}^s is the component of the theoretical Piola–Kirchhoff measure, that is the tensor that conjugates with the theoretical deformation gradient in the sense of mechanical work. Nevertheless, spatial measures such as the Cauchy stress are often preferred in the context of constitutive modeling.

3.2.3. Consistent eulerian stress

The symmetric velocity gradient $\mathbf{d} = \text{sym}(\dot{\mathbf{F}} \mathbf{F}^{-\top})$ is the eulerian kinematic quantity of interest. In the following developments, the simple shear contribution to this velocity gradient is isolated, and the corresponding conjugate stress identified. A push forward can be applied to expression (29) to write the power of internal forces on a material element of the current configuration $d\Omega$ using spatial quantities:

$$p_i = \boldsymbol{\sigma} : (\dot{\mathbf{F}} \mathbf{F}^{-\top}). \quad (32)$$

This is equivalent to the conventional writing $(\boldsymbol{\sigma} : \mathbf{d})$ since only the symmetric parts of the right operands are multiplied. Introducing the decomposition $\mathbf{F} = \mathbf{F}^* \mathbf{F}^s$, then isolating $\mathbf{d}^s = \text{sym}(\dot{\mathbf{F}}^s \mathbf{F}^{s-\top})$, leads to

$$p_i = \underbrace{\boldsymbol{\sigma} : (\dot{\mathbf{F}}^* \mathbf{F}^{*-1})}_{p_i^*} + \underbrace{\text{skew}(\mathbf{F}^{*\top} \boldsymbol{\sigma} \mathbf{F}^{*-1}) : \text{skew}(\dot{\mathbf{F}}^s \mathbf{F}^{s-\top})}_{\mathbf{w}^s} + \underbrace{\text{sym}(\mathbf{F}^{*\top} \boldsymbol{\sigma} \mathbf{F}^{*-1}) : \text{sym}(\dot{\mathbf{F}}^s \mathbf{F}^{s-\top})}_{p_i^s} \quad (33)$$

In this expression, \mathbf{d}^s and \mathbf{w}^s respectively represent the symmetric part and the skew-symmetric part of the theoretical velocity gradient. Developing the theoretical contribution to the power of internal forces taking an arbitrary stress state $\boldsymbol{\sigma} = \sigma_{ij} \mathbf{e}_i \otimes \mathbf{e}_j$ brings:

$$p_i^s = \underbrace{\frac{u_1 + u_2}{2u_1u_2} (\sigma_{21}(\cos^2 \mu - \sin^2 \mu) + (\sigma_{11} - \sigma_{22}) \cos \mu \sin \mu)}_{\sigma_{21}^s} \dot{\gamma}_{2d_{21}^s} \quad (34)$$

This expression reduces to the conventional writing, $p_i = 2\sigma_{21}d_{21}$, in the absence of unwanted deformations. Otherwise, it can be seen as a way to adjust the experimental results by enforcing the consistency of strains and stresses. It must be based on the measurement and partition of the deformation gradient.

3.2.4. Momentum balance

In the present section, the developments of section 3.2.1 are rewritten without postulating perfect alignment or ideal kinematics. A correction factor is derived using information provided by field measurement techniques. The starting point for constitutive identification is the vertical section momentum balance presented in section 3.2.1.

$$\mathbf{f} = \mathbf{e}_2 \int_A \boldsymbol{\sigma} \mathbf{e}_1 \, dA = \int_A \sigma_{21} \, dA. \quad (35)$$

This integral is performed in the spatial configuration, therefore there is no guaranty that it follows any material direction. Moreover, its numerical handling is not direct since it requires interpolations on the moving grid of material points that DIC provides. Let us apply a pull back to the reference configuration: the integration now applies over the first Piola–Kirchhoff stress $\mathbf{J}\boldsymbol{\sigma}\mathbf{F}^{-\top}$.

$$\mathbf{f} = \int_{A_0} F_{22}^m \sigma_{21} \, dA_0. \quad (36)$$

Note that the assumption of ideal kinematics is not made since field measurement results are used. This integral applies over a material subdomain, hence its better consistency with characterization and ease of computation given a DIC grid. The deformation gradient component is substituted with its decomposition

$F_{22}^m = u_2 \cos \mu$ from (19). The total stress is also written as a function of the theoretical stress using (34).

$$f = \int_{A_0} \chi(\mathbf{F}) \sigma_{21}^s dA_0 \quad (37)$$

$$\text{where } \chi(\mathbf{F}) = \frac{2u_1 u_2^2 \cos \mu}{(u_1 + u_2)(\cos^2 \mu - \sin^2 \mu)}. \quad (38)$$

This writing ensures that the identified stress is consistent with the computed kinematic measures. It is represented by the factor $\chi(\mathbf{F})$ that reduces to 1 in case of no unwanted deformation. Using the usual homogeneity assumption, it can provide a minor correction to the computed stress measure.

185 4. Results and discussion

In order to set a reference that is used throughout the paper to compare different setups, let the average shear Γ be defined as:

$$\Gamma = \int_{-\alpha h/2}^{\alpha h/2} F_{21} dX_1 \quad (39)$$

where h is the width of the gauge zone (horizontal directions in figure 2), and α a chosen coefficient. In the above expression, the center of the gauge zone is taken at $(X_1 = 0, X_2 = 0)$. The length ratio α is taken equal to 0.75 in order to avoid issues linked to the loss of data at the gauge zone edges. The average shear is used in place of the grips displacement that can critically loose local significance for pseudo-shear.

190 4.1. Shear parameter identification

Figure 6 presents several shear parameter estimates as a function of the normalized testing time of two samples: simple (left) and pseudo-shear (right). The estimates are based on several measures: the raw deformation gradient (F_{21} , equation (2)); the Green–Lagrange strain (E_{11}, E_{12} , expression (4)), and its eigenvalues ($E_i = (C_i - 1)/2$, expressions (6) and (7)). The last set of points is deduced from the decomposition (19). These data are taken from the subset corresponding to the middle of the sample, with no addition smoothing or averaging.

Since the effective deformation always deviates from theoretical simple shear, each approach yields a different result. The overall relative dispersion reaches up to 20 %: up to 0.1 in simple shear and 0.4 in pseudo-shear that reaches much higher strains. Such a difference is notable and inherent to shear testing: it may not be significantly reduced by acting on the experimental setup or equipments. This scattering of results justifies the necessity of a reliable definition as proposed in equation (20), that is consistent with the characterization purpose and invariant with respect to the precision of the setup.

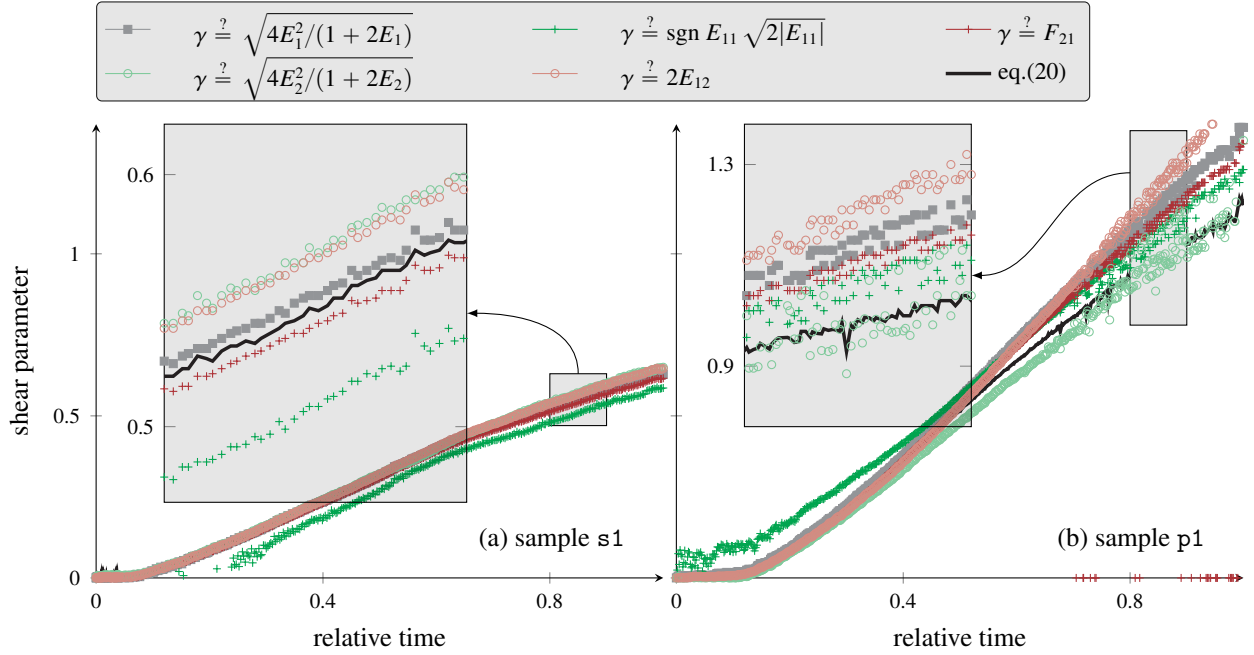


Figure 6: Comparison of different shear parameter estimates at the center of the gauge zone for one simple shear test and one pseudo-shear test. A significant dispersion is due to the fact that the actual deformation always slightly deviates from the ideal simple shear.

4.2. Deviation from simple shear

A classical way to check the deviation from simple shear is to compare the eigenvalues of the measured spatial Hencky strain. If they are equal in magnitude and opposite in sign, then the deformation taking place is simple shear as written in expression (17). But this approach suffers from two disadvantages that are solved by the proposed method; they are both due to disregarding the orientation of the eigenbasis. While equal and opposite eigenvalues guaranty shear, they do not hold any information about the direction of the deformation, hence the right load type might take place in the wrong material orientation. This is an issue when characterizing anisotropic materials. Moreover, a deviation from equal and opposite eigenvalues means plane stretches that may not be characterized in the absence of information about eigenvectors. In this section, the stretches of decomposition (19) are used to quantify the importance of the unwanted deformation.

Note that the rotation \mathbf{R} (from the polar decomposition) given in (15) indicates that the material frame itself rotates continuously (and non-proportionally) as simple shear proceeds. As emphasized by Chen et al. (2018) and Abedini et al. (2020), this causes the eigenbasis of any strain or stress measure to reorient with

plastic deformation. It does so regardless of the initial orientation and forbids any material alignment to be conserved or controlled.

220 A comparison between the four considered geometries is performed in figure 7. For the sake of consistency, the global estimate of the shear parameter is fixed at $\Gamma = 0.5$ for all tests. Therefore the presented figures are only snapshots and the reported quantities vary with the deformation.

225 The figure is composed of four regions corresponding to each geometry. On the top of each region, a colored map gives the spatial distribution of the order of magnitude (decimal logarithm) of the error on the DIC region shown in figure 2. The error is taken as the Frobenius norm of the difference between the unwanted stretch and unity: $\|U^* - I\|$. It corresponds to a kinematic distance from simple shear. The middle shearing axis X_2 is added on each map as a white dashed line. On the bottom, each component of the deformation gradient is plotted along the middle axis. The deviation from ideal kinematics can be observed as the vertical distance between each point and the theoretically homogeneous state represented by $F_{11} = F_{22} = 1$, $F_{21} = 0.5$ and $F_{12} = 0$.

230 It can first be observed that the error magnitude is overall slightly higher on pseudo-shear tests. It can be understood by noticing darker shades on the error maps of figure 7, or more clearly by looking at the distance between the measured deformation gradient components and their theoretical value of 0, 0.5 or 1. This is consistent with the fact that resulting shear forces are imposed rather than shear kinematics. The error tends to stabilize in the middle of the samples and rises up to significance (0.1) at their edges. In an
235 similar way, the components of the deformation gradient remain stable in the center of the sample and loose homogeneity at the left and right limits. This is due to the free edges of the samples that imply null stresses, hence forbid shear. The order of magnitude of both components u_1 and u_2 remains equal throughout the deformation.

240 Another problematic is illustrated in figure 7-s2 where the deformation gradient is visibly asymmetric. A probable cause lies in a default of alignment between the machine and the DIC approximation basis. It may not be easily solved during postprocessing since the misalignment may change as the test proceeds. For example, in the present case, the slight rotation of the device occurred shortly after the beginning of the test. While the pseudo-shear tests appear larger due to their aspect ratio, their smaller gauge region implies fewer data. Because of their greater accuracy and more available data, simple shear tests appear
245 more reliable to recreate the ideal kinematics of shear testing.

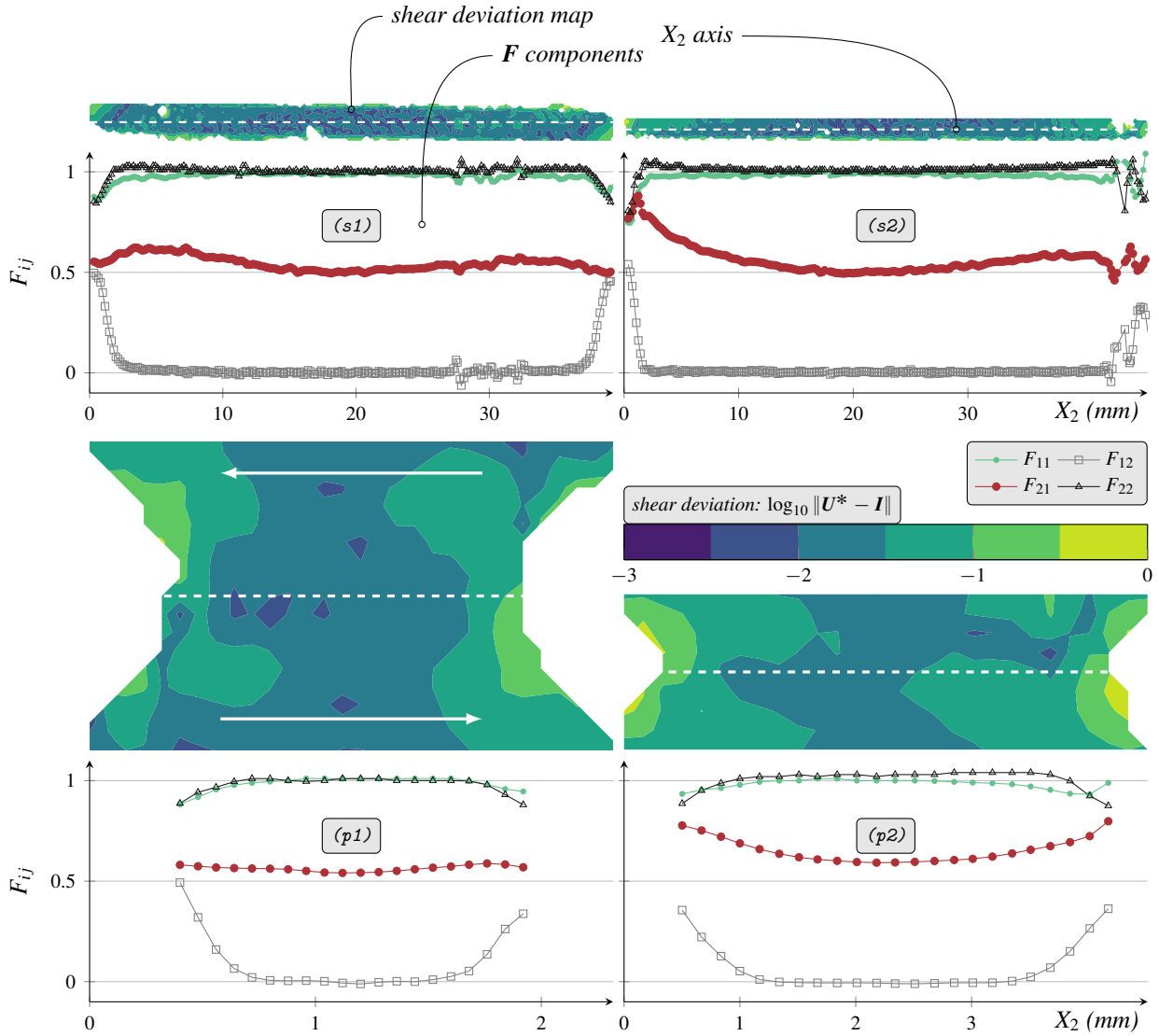


Figure 7: Snapshots of the unwanted strains and deformation gradient components for the four different samples at $\Gamma = 0.5$. The figure is divided into four regions presenting: on top, the shear error map and the longitudinal X_2 axis; on the bottom, the deformation gradient components distribution along the axis. The aspect ratios of the images are conserved: the simple shear maps appear much smaller because of the slenderness of their geometry. The “error” measure is chosen as the order of magnitude of the norm of the difference between the unwanted stretches U^* and identity.

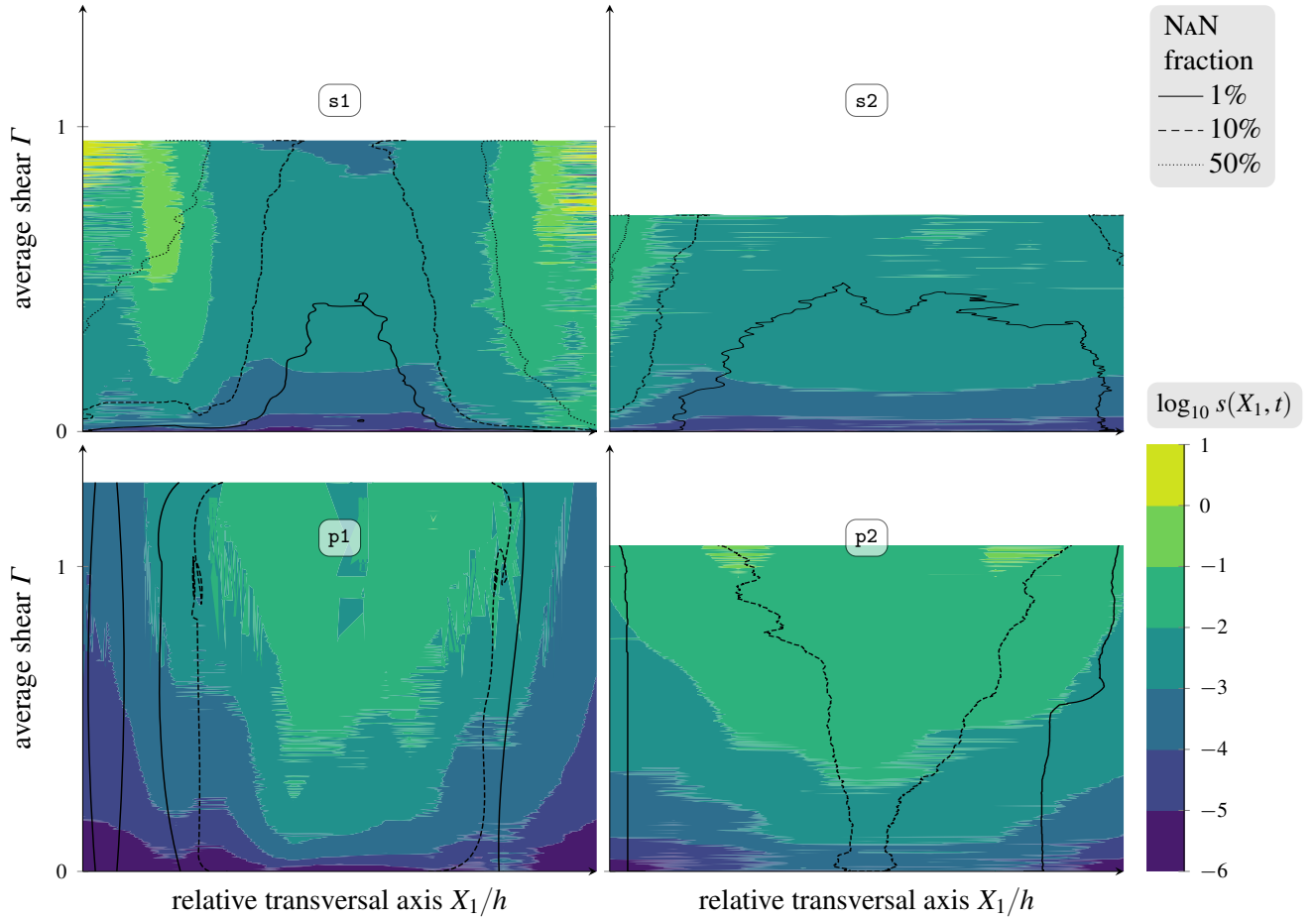


Figure 8: Heterogeneity factor maps for the four different samples. The factor s defined in (24) is the spacial standard deviation of the shear parameter integrated along the loading direction (X_2). Its order of magnitude is given along the transversal direction (X_1) for the whole test duration represented by the increasing average shear Γ defined in (39). The topological lines represent the amount of unavailable data (NaN fraction). In an ideal test, both the NaN fraction and the homogeneity factor would be null at all instant in the middle section.

4.3. Heterogeneity

In figure 8, the order of magnitude (decimal logarithm) of the heterogeneity factor s from equation (24) is represented as a colored map function of space (X_1) and average shear (I) for each of the four considered sample types. The color of each point of the maps thus gives a measure of the heterogeneity of the corresponding longitudinal section, at the corresponding instant. Understandably, heterogeneity is lower at the bottom of the graphs, that is the beginning of the tests; and increases monotonously with shear intensity.

An additional set of data named “not a number (NaN) fraction” is added on each plot in the form of isolines. It gives the proportion of points which do not hold a value when the DIC algorithm diverges. This can be interpreted as a ratio of length that has to be extrapolated for the remaining data: an increase of this value necessarily decreases the results credence. It is systematic as a test proceeds and distortions intensify.

Simple shear tests s1 and s2 show an increase in heterogeneity at the edges of the sample, which corresponds to a lack of measuring precision induced by the presence of grips. Both the NaN fraction and heterogeneity factor show a better quality at the center of the sample. The opposite is observed for pseudo-shear tests p1 and p2 where measurements tend to increase in quality and homogeneity as they are performed far from the center. It can be problematic since the mechanical state is less clearly defined on the sides of the pseudo-shear gauge zone, where the loading path mixes tension and shear.

In quantitative terms, the homogeneity is better by up to an order of magnitude for simple shear tests. This is likely due to the length ratio that is always more favorable in simple shear. In conclusion for the considered material and four geometries, the exact middle of the sample is a natural choice for post processing. It should be chosen either to measure an average strain or to apply the momentum balance on a vertical cross-section (section 3.2.1).

4.4. Stress correction

Equation (34) features the shear component σ_{21}^s of the Cauchy-like stress measure that conjugates with the theoretical shear strain rate. This corresponds to a fictitious configuration where unwanted deformations are canceled. Using the standard assumption for the measured stress allows to use definitions (26) and (28). Then the coefficient $(1 - \sigma_{21}^s/\tau)$ can be seen as the proportion of stress that works in the unwanted motion.

This factor is shown in figure 9 where simple shear trends (left hand side) are compared to pseudo-shear (right hand side). It can be seen that the distance increases with increasing strains, specifically in the case of pseudo-shear where shear kinematics are not explicitly prescribed. This error can reach several

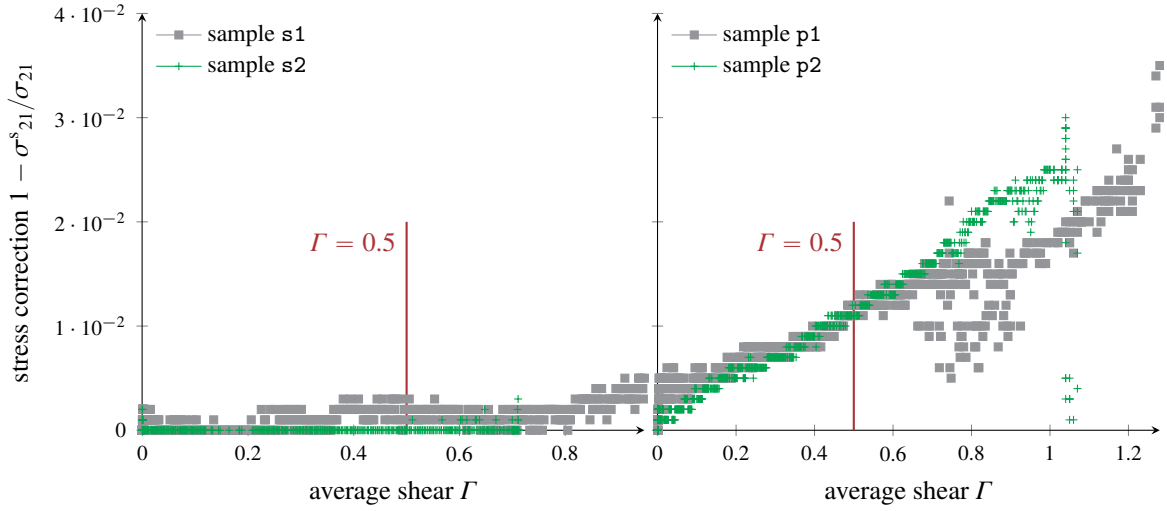


Figure 9: Relative difference between theoretical and measured shear stresses. The factor can be seen as a correction applied on the total stress to remove the part that conjugates with the unwanted deformation.

percents which can be significant in the context of a thorough characterization. These values correspond to an order of magnitude that can be improved or worsened depending on the experimental setup precision. The stiffness of the simple shear setup nonetheless ensures small deviations throughout the experimental campaign.

280 4.5. Work-hardening

Figure 10 compares typical work-hardening curves obtained for each of the four sample types, and provides a reference tensile test in the rolling direction. The equivalent stress is computed as the von Mises norm $\bar{\sigma} = \sqrt{3/2} \|\text{dev } \boldsymbol{\sigma}\|$. The corresponding strain $\bar{\epsilon}$ is integrated to satisfy the plastic work equivalence:

$$\bar{\sigma} \dot{\bar{\epsilon}} = \boldsymbol{\sigma} : \dot{\mathbf{h}}^p \quad (40)$$

where $\dot{\mathbf{h}}^p$ is the plastic strain. Its component are obtained using the theoretical shear parameter (20) and the spatial Hencky tensor (18) neglecting elastic strains. A similar comparison is proposed by H erault et al. (2021). The same material is used and work-hardening data are also compared using von Mises equivalent stress.

285 Among shear tests, a difference of up to 2 % can be observed among similar geometries (s1–s2 or p1–p2) while simple shear can differ from pseudo-shear by up to 8 % in terms of stress magnitude at fixed strains. Therefore the present approach does not suffice to unify results from different loading techniques.

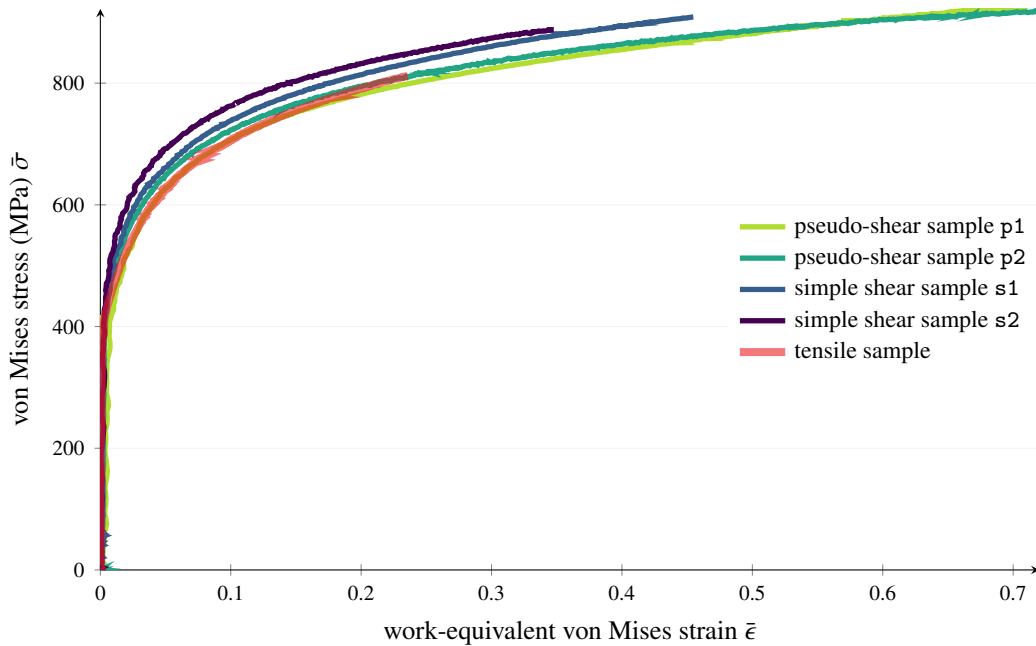


Figure 10: Work-hardening results after shear (p1, p2, s1, s2) and tensile tests in the rolling direction. The plots stop when fracture (or necking) is reported on the shear (or tensile) sample.

Since kinematic assumptions are here removed, it appears that a finer evaluation of the stress tensor field is needed to further converge.

290 5. Conclusions

Owing to field measurements methods, this work aims to assess and improve the performance of the characterization of sheet metals under shear. After a thorough recall of the kinematics of simple shear, the deviation from theory to experiments is quantified in terms of tensorial direction and heterogeneity. Then the experimental biases are taken into account to derive stress measures that consistently conjugate with
 295 the theoretical shear strain. This way, the unavoidable experimental errors can be accounted for during post-processing.

The theory is applied to four types of tests performed on dual phase steel sheets. Heterogeneity and deviation factors are used to compare the quality of the experimental implementations, and an identification of the shear parameter is performed while avoiding the emphasized biases. A DIC-based correction factor
 300 is also proposed to adjust the stress results.

The main contributions of this work can be emphasized as follows.

(i) An unambiguous definition of the shear parameter is proposed by splitting the effective deformation gradient into theoretical and *unwanted* contributions.

(ii) The corresponding stress measures are provided for the consistency of post-processing.

305 (iii) Estimates of measurement errors and quality are defined in the form of heterogeneity factors and unwanted deformations components. They enable the quantitative comparison of the quality of tests.

The kinematic decomposition can be straight-forwardly extended to any plane state experimental testing procedure to lift ambiguities in kinematics postprocessing. It is here emphasized that, for the considered material and specimens, simple shear is in general more reliable than pseudo-shear, even though the latter is
310 unavoidable in cases such as fracture characterization. The measured deviations remain largely acceptable and do not disqualify any technology on the whole.

The remaining hypotheses that require attention and improvements concern the stress states. The components of forces perpendicular to the shear direction can be measured given a supplementary experimental effort (G' Sell et al., 1983). Nevertheless, the variations of stress along the shear direction remain an unre-
315 solved challenge towards the complete characterization in shear. In this context, rather than seeking more comprehensive data, one may improve their analytical treatment: this is the approach exemplified in the present work. The third type of improvement is computational and could lie, for example, in non parametric measurements such as data-driven identification (Leygue et al., 2019).

Acknowledgment

320 The authors thank Anthony Jegat, Hervé Bellegou and Ludovic Kiatkowski who took part in the experimental investigations. The first author thanks Adrien Vinel (orcid.org/0000-0002-6167-1823) for his participation in the analytical verification of section 3.1.1.

Appendix A. Shear deformation identities

The following identities are, if not trivial to the reader, useful when expanding definitions in order to obtain the results summarized in section 3.1.1.

$$\sqrt{\frac{\gamma}{2} \left| \gamma \pm \sqrt{4 + \gamma^2} \right| + 1} = \frac{1}{2} \left| \gamma \pm \sqrt{4 + \gamma^2} \right|, \quad (\text{A.1})$$

$$\frac{1}{2} \left(\gamma \pm \sqrt{4 + \gamma^2} \right)^2 - 4 = \gamma \left(\gamma \pm \sqrt{4 + \gamma^2} \right), \quad (\text{A.2})$$

$$\frac{1}{2} \left(\gamma \pm \sqrt{4 + \gamma^2} \right)^2 + 4 = \sqrt{4 + \gamma^2} \left(\gamma \pm \sqrt{4 + \gamma^2} \right). \quad (\text{A.3})$$

References

- 325 A. Abedini, C. Butcher, and M. J. Worswick. Fracture characterization of rolled sheet alloys in shear loading: Studies of specimen geometry, anisotropy, and rate sensitivity. *Experimental Mechanics*, 57(1):75–88, September 2016. doi: 10.1007/s11340-016-0211-9.
- A. Abedini, C. Butcher, M. J. Nemcko, S. Kurukuri, and M. J. Worswick. Constitutive characterization of a rare-earth magnesium alloy sheet (ZEK100-o) in shear loading: Studies of anisotropy and rate sensitivity. *International Journal of Mechanical*
330 *Sciences*, 128-129:54–69, August 2017. doi: 10.1016/j.ijmecsci.2017.04.013.
- A. Abedini, C. Butcher, T. Rahman, and M. J. Worswick. Evaluation and calibration of anisotropic yield criteria in shear loading: constraints to eliminate numerical artefacts. *International Journal of Solids and Structures*, 151:118–134, 2018. ISSN 0020-7683. doi: 10.1016/j.ijsolstr.2017.06.029. URL <http://www.sciencedirect.com/science/article/pii/S0020768317303013>. Special Issue with a Selection of
335 Papers from the NUMISHEET 2016 Conference.
- A. Abedini, J. Noder, C. P. Kohar, and C. Butcher. Accounting for shear anisotropy and material frame rotation on the constitutive characterization of automotive alloys using simple shear tests. *Mechanics of Materials*, 148:103419, September 2020. doi: 10.1016/j.mechmat.2020.103419.
- Y. G. An, H. Vegter, and J. Heijne. Development of simple shear test for the measurement of work hardening. *Journal of*
340 *Materials Processing Technology*, 209(9):4248–4254, 2009. ISSN 0924-0136. doi: 10.1016/j.jmatprotec.2008.11.007. URL <https://www.sciencedirect.com/science/article/pii/S0924013608007437>.
- ASTM. *Standard test method for shear testing of thin aluminum alloy products*. 2019. doi: 10.1520/B0831-19. URL <http://www.astm.org/cgi-bin/resolver.cgi?B831>.
- Frédéric Barlat, Seong-Yong Yoon, Shin-Yeong Lee, Min-Su Wi, and Jin-Hwan Kim. Distortional plasticity framework with appli-
345 cation to advanced high strength steel. *International Journal of Solids and Structures*, 202:947–962, 2020. ISSN 0020-7683. doi: 10.1016/j.ijsolstr.2020.05.014. URL <http://www.sciencedirect.com/science/article/pii/S0020768320301827>.
- S. Bouvier, H. Haddadi, P. Levée, and C. Teodosiu. Simple shear tests: Experimental techniques and characterization of the plastic anisotropy of rolled sheets at large strains. *Journal of Materials Process-*

- ing *Technology*, 172(1):96–103, 2006. ISSN 0924-0136. doi: 10.1016/j.jmatprotec.2005.09.003. URL
350 <http://www.sciencedirect.com/science/article/pii/S092401360500823X>.
- A. Brosius, Q. Yin, A. Güner, and A. E. Tekkaya. A new shear test for sheet metal characterization. *Steel research international*, 82(4):323–328, 2011. doi: 10.1002/srin.201000163.
- C. Butcher and A. Abedini. Shear confusion: identification of the appropriate equivalent strain in simple shear using the logarithmic strain measure. *International Journal of Mechanical Sciences*, 134:273–283, 2017. ISSN 0020-7403. doi:
355 10.1016/j.ijmecsci.2017.10.005. URL <http://www.sciencedirect.com/science/article/pii/S0020740317320817>.
- J. Carbonnière, S. Thuillier, F. Sabourin, M. Brunet, and P. Y. Manach. Comparison of the work hardening of metallic sheets in bending–unbending and simple shear. *International Journal of Mechanical Sciences*, 51(2):122–130, 2009. ISSN 0020-7403. doi: 10.1016/j.ijmecsci.2008.12.006. URL
<https://www.sciencedirect.com/science/article/pii/S0020740308001811>.
- 360 Kelin Chen, Stelios Kyriakides, and Martin Scales. Effect of material frame rotation on the hardening of an anisotropic material in simple shear tests. *Journal of Applied Mechanics*, 85(12), September 2018. doi: 10.1115/1.4041320.
- J. Courbon and J. L. Duval. Strain hardening of aluminium alloy 3004 in the deep drawing and ironing processes. *Le Journal de Physique IV*, 03(C7):C7–247–C7–250, November 1993. doi: 10.1051/jp4:1993739.
- M. Destrade, J. G. Murphy, and G. Saccomandi. Simple shear is not so simple. *International Journal of*
365 *Non-Linear Mechanics*, 47(2):210–214, 2012. ISSN 0020-7462. doi: 10.1016/j.ijnonlinmec.2011.05.008. URL
<http://www.sciencedirect.com/science/article/pii/S0020746211001065>. Nonlinear Continuum Theories.
- Christian G’ Sell, Serge Boni, and Suresh Shrivastava. Application of the plane simple shear test for determination of the plastic behaviour of solid polymers at large strains. *Journal of Materials Science*, 18(3):903–918, March 1983. ISSN 1573-4803. doi: 10.1007/BF00745590.
- 370 R. Garcia, T. A. Weisshaar, and R. R. McWithey. An experimental and analytical investigation of the rail shear-test method as applied to composite materials. *Experimental Mechanics*, 20(8):273–279, August 1980. ISSN 1741-2765. doi: 10.1007/BF02328411.
- Diane Hérault, Sandrine Thuillier, Shin-Yeong Lee, Pierre-Yves Manach, and Frédéric Barlat. Calibration of a strain path change model for a dual phase steel. *International Journal of Mechanical Sciences*, 194:106217, 2021. ISSN 0020-7403. doi:
375 10.1016/j.ijmecsci.2020.106217. URL <http://www.sciencedirect.com/science/article/pii/S0020740320343228>.
- Akhtar S. Khan, Amit Pandey, Thomas Gnäupel-Herold, and Raja K. Mishra. Mechanical response and texture evolution of AZ31 alloy at large strains for different strain rates and temperatures. *International Journal of Plasticity*, 27(5):688–706, 2011. ISSN 0749-6419. doi: 10.1016/j.ijplas.2010.08.009. URL
<http://www.sciencedirect.com/science/article/pii/S0749641910001142>.
- 380 Amit Kumar, M. K. Singha, and Vikrant Tiwari. Structural response of metal sheets under combined shear and tension. *Structures*, 26:915–933, August 2020. doi: 10.1016/j.istruc.2020.05.006.
- Adrien Leygue, Rian Seghir, Julien Réthoré, Michel Coret, Erwan Verron, and Laurent Stainier. Non-parametric material state field extraction from full field measurements. *Computational Mechanics*, 64(2):501–509, 2019.
- Yanshan Lou, Saijun Zhang, and Jeong Whan Yoon. Strength modeling of sheet metals from shear to plane strain tension. *Inter-*
385 *national Journal of Plasticity*, 134:102813, November 2020. doi: 10.1016/j.ijplas.2020.102813.
- P. Y. Manach, S. Thuillier, J. W. Yoon, J. Coër, and H. Laurent. Kinematics of Portevin–Le Chatelier bands in simple shear.

International Journal of Plasticity, 58:66–83, July 2014. doi: 10.1016/j.ijplas.2014.02.005.

- Z. Marciniak and J. Kolodziejski. Assessment of sheet metal failure sensitivity by method of torsioning the rings. In *Proceedings of the 7th biannual congress of the IDDRG*, pages 61–64, 1972.
- 390 M. Mazière, C. Luis, A. Marais, S. Forest, and M. Gaspérini. Experimental and numerical analysis of the Lüders phenomenon in simple shear. *International Journal of Solids and Structures*, 106-107:305–314, February 2017. doi: 10.1016/j.ijsolstr.2016.07.026.
- K. Miyachi. A proposal of a planar simple shear. *Journal of Materials Science*, 18:903–918, 1977.
- D. Mohr and S. Henn. A new method for calibrating phenomenological crack formation criteria. *Impact and Crashworthiness Laboratory Report*, 113, 2004.
- 395 D. Mohr and S. Henn. Calibration of stress-triaxiality dependent crack formation criteria: A new hybrid experimental–numerical method. *Experimental Mechanics*, 47(6):805–820, February 2007. doi: 10.1007/s11340-007-9039-7.
- D. C. Moreira and L. C. S. Nunes. Comparison of simple and pure shear for an incompressible isotropic hyperelastic material under large deformation. *Polymer Testing*, 32(2):240–248, April 2013. doi: 10.1016/j.polymertesting.2012.11.005.
- 400 A. F. G. Pereira, P. A. Prates, M. C. Oliveira, and J. V. Fernandes. Normal stress components during shear tests of metal sheets. *International Journal of Mechanical Sciences*, 164:105169, 2019. ISSN 0020-7403. doi: 10.1016/j.ijmecsci.2019.105169. URL <https://www.sciencedirect.com/science/article/pii/S0020740318341389>.
- C. H. Pham, F. Adzima, J. Coër, and P. Y. Manach. Anti-buckling device for ultra-thin metallic sheets under large and reversed shear strain paths. *Experimental Mechanics*, 57(4):593–602, February 2017. doi: 10.1007/s11340-017-0256-4.
- 405 E. F. Rauch. Plastic anisotropy of sheet metals determined by simple shear tests. *Materials Science and Engineering: A*, 241(1):179–183, 1998. ISSN 0921-5093. doi: 10.1016/S0921-5093(97)00486-3. URL <http://www.sciencedirect.com/science/article/pii/S0921509397004863>.
- E. F. Rauch and C. G’Sell. Flow localization induced by a change in strain path in mild steel. *Materials Science and Engineering: A*, 111:71–80, 1989. ISSN 0921-5093. doi: 10.1016/0921-5093(89)90199-8. URL
- 410 <http://www.sciencedirect.com/science/article/pii/0921509389901998>.
- A. Reyes, M. Eriksson, O.-G. Lademo, O. S. Hopperstad, and M. Langseth. Assessment of yield and fracture criteria using shear and bending tests. *Materials & Design*, 30(3):596–608, 2009. ISSN 0261-3069. doi: 10.1016/j.matdes.2008.05.045. URL <http://www.sciencedirect.com/science/article/pii/S0261306908002239>.
- Christian C. Roth and Dirk Mohr. Ductile fracture experiments with locally proportional loading histories. *International Journal of Plasticity*, 79:328–354, 2016. ISSN 0749-6419. doi: 10.1016/j.ijplas.2015.08.004. URL
- 415 <http://www.sciencedirect.com/science/article/pii/S0749641915001412>.
- Christian C. Roth and Dirk Mohr. Determining the strain to fracture for simple shear for a wide range of sheet metals. *International Journal of Mechanical Sciences*, 149:224–240, December 2018. doi: 10.1016/j.ijmecsci.2018.10.007.
- David Salomon. *The computer graphics manual*. Springer London, 2011. doi: 10.1007/978-0-85729-886-7.
- 420 D. R. Shouler and J. M. Allwood. Design and use of a novel sample design for formability testing in pure shear. *Journal of Materials Processing Technology*, 210(10):1304–1313, 2010. ISSN 0924-0136. doi: 10.1016/j.jmatprotec.2010.03.019. URL <http://www.sciencedirect.com/science/article/pii/S0924013610000981>.
- B. Starman, M. Vrh, P. Koc, and M. Halilović. Shear test-based identification of hardening behaviour of stainless steel sheet after onset of necking. *Journal of Materials Processing Technology*, 270:335–344, August 2019. doi:

425 10.1016/j.jmatprotec.2019.03.010.

Christian Thiel, Jendrik Voss, Robert J. Martin, and Patrizio Neff. Shear, pure and simple. *International Journal of Non-Linear Mechanics*, 112:57–72, 2019. ISSN 0020-7462. doi: 10.1016/j.ijnonlinmec.2018.10.002. URL <http://www.sciencedirect.com/science/article/pii/S0020746218304116>.

430 S. Thuillier and P. Y. Manach. Comparison of the work-hardening of metallic sheets using tensile and shear strain paths. *International Journal of Plasticity*, 25(5):733–751, 2009. ISSN 0749-6419. doi: 10.1016/j.ijplas.2008.07.002. URL <http://www.sciencedirect.com/science/article/pii/S0749641908001101>.

H. Vegter and A. H. van den Boogaard. A plane stress yield function for anisotropic sheet material by interpolation of biaxial stress states. *International Journal of Plasticity*, 22(3):557–580, March 2006. doi: 10.1016/j.ijplas.2005.04.009.

435 Z. J. Wang, L. H. Zheng, and Z. Wang. Characterization of forming limits at fracture for aluminum alloy 6k21-t4 sheets in non-linear strain paths using a biaxial tension/shear loading test. *International Journal of Mechanical Sciences*, 184:105672, October 2020. doi: 10.1016/j.ijmecsci.2020.105672.

Q. Yin, C. Soyarslan, A. Güner, A. Brosius, and A. E. Tekkaya. A cyclic twin bridge shear test for the identification of kinematic hardening parameters. *International Journal of Mechanical Sciences*, 59(1):31–43, 2012. ISSN 0020-7403. doi: 10.1016/j.ijmecsci.2012.02.008. URL <http://www.sciencedirect.com/science/article/pii/S0020740312000458>.

440 Q. Yin, C. Soyarslan, K. Isik, and A. E. Tekkaya. A grooved in-plane torsion test for the investigation of shear fracture in sheet materials. *International Journal of Solids and Structures*, 66:121–132, 2015. ISSN 0020-7683. doi: 10.1016/j.ijsolstr.2015.03.032. URL <http://www.sciencedirect.com/science/article/pii/S002076831500164X>.

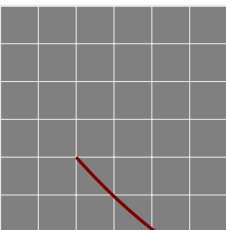
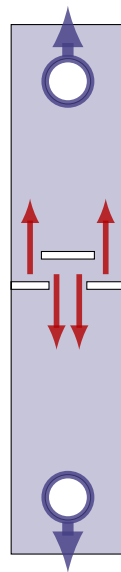
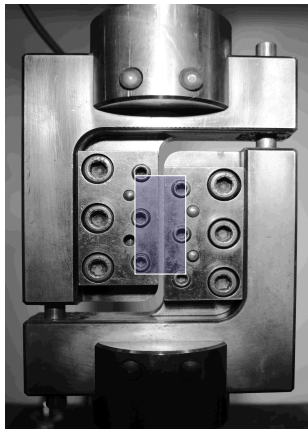
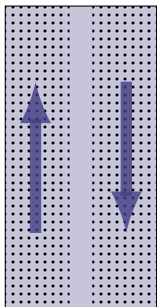
Qing Yin, Benjamin Zillmann, Sebastian Suttner, Gregory Gerstein, Manfredi Biasutti, A. Erman Tekkaya, Martin F.-X. Wagner, Marion Merklein, Mirko Schaper, Thorsten Halle, and Alexander Brosius. An experimental and numerical investigation of different shear test configurations for sheet metal characterization. *International Journal of Solids and Structures*, 51(5):1066–1074, 2014. ISSN 0020-7683. doi: 10.1016/j.ijsolstr.2013.12.006. URL <http://www.sciencedirect.com/science/article/pii/S0020768313004794>.

450 S. L. Zang, S. Thuillier, A. Le Port, and P. Y. Manach. Prediction of anisotropy and hardening for metallic sheets in tension, simple shear and biaxial tension. *International Journal of Mechanical Sciences*, 53(5):338–347, 2011. ISSN 0020-7403. doi: 10.1016/j.ijmecsci.2011.02.003. URL <http://www.sciencedirect.com/science/article/pii/S002074031100035X>.

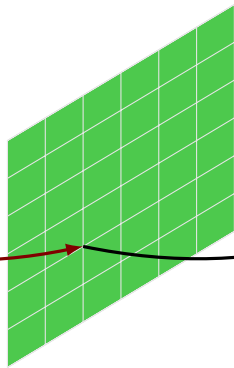
Peng Zhang, Michael P. Pereira, Buddhika Abeyrathna, Bernard F. Rolfe, Daniel E. Wilkosz, and Matthias Weiss. Improving the shear test to determine shear fracture limits for thin stainless steel sheet by shape optimisation. *International Journal of Mechanical Sciences*, 164:105116, December 2019. doi: 10.1016/j.ijmecsci.2019.105116.

455 X. Zhou and K. K. Tamma. On the applicability and stress update formulations for corotational stress rate hypoelasticity constitutive models. *Finite Elements in Analysis and Design*, 39(8):783–816, 2003. ISSN 0168-874X. doi: 10.1016/S0168-874X(03)00059-3. URL <http://www.sciencedirect.com/science/article/pii/S0168874X03000593>. 14th Robert J. Melosh Competition.

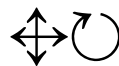
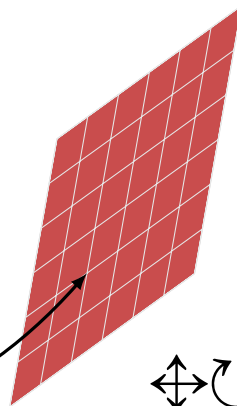
(pseudo-)simple shear



from theory



?



to experiments